

Voltage-Controlled Anisotropy and Current-Induced Magnetization Dynamics in Antiferromagnetic-Piezoelectric Layered Heterostructures

P.A. Popov^{1,2,*}, A.R. Safin^{1,3,†}, A. Kirilyuk^{1,4,5}, S.A. Nikitov^{1,2,6}, I. Lisenkov⁷, V. Tyberkevich⁸,
and A. Slavin⁸

¹*Kotel'nikov Institute of Radio-Engineering and Electronics of RAS, Moscow 125009, Russia*

²*Moscow Institute of Physics and Technology, Dolgoprudny 141701, Moscow Region, Russia*

³*Moscow Power Engineering Institute, Moscow 111250, Russia*


⁴*Institute for Molecules and Materials, Radboud University, 6525 AJ Nijmegen, Netherlands*

⁵*FELIX Laboratory, Radboud University, 6525 AJ Nijmegen, Netherlands*

⁶*Laboratory "Metamaterials", Saratov State University, Saratov 410012, Russia*

⁷*Winchester Technologies LLC, Burlington, Massachusetts 01803, USA*

⁸*Department of Physics, Oakland University, Rochester, Michigan 48309-4479, USA*

 (Received 21 January 2020; revised manuscript received 19 February 2020; accepted 31 March 2020; published 30 April 2020; corrected 17 November 2020)

It is shown theoretically that in a layered heterostructure comprising piezoelectric, dielectric antiferromagnetic crystal, and heavy metal (PZ/AFM/HM), it is possible to control the anisotropy of the AFM layer by applying a dc voltage across the PZ layer. In particular, we show that by varying the dc voltage across the heterostructure and/or the dc current in the HM, it is possible to vary the frequency of the antiferromagnetic resonance of the AFM in a passive (subcritical) regime and, also, to reduce the threshold of the current-induced terahertz-frequency generation. Our analysis also shows that, unfortunately, the voltage-induced reduction of the generation threshold leads to the proportional reduction of the amplitude of the terahertz-frequency signal generated in the active (supercritical) regime. The general results are illustrated by a calculation of the characteristics of experimentally realizable PZT-5H/NiO/Pt.

DOI: [10.1103/PhysRevApplied.13.044080](https://doi.org/10.1103/PhysRevApplied.13.044080)

I. INTRODUCTION

In the recent years, antiferromagnetic (AFM) spintronics has attracted considerable attention from researchers [1,2]. Antiferromagnets are interesting for spintronic applications because the magnetic order in these substances does not require an external bias magnetic field, as it is supported by a very large internal magnetic field of an exchange nature, which, along with the moderate magnetic field of the AFM anisotropy, determines the frequency of the antiferromagnetic resonance (AFMR) lying in the subterahertz to terahertz frequency range [3–6]. Thus, AFMs can be considered as promising materials for the development of signal generators operating in the terahertz frequency range.

It has been shown previously [7–9] that spin-torque nano-oscillators (STNOs) driven by a spin-transfer torque and based on ferromagnets (FMs) can generate signals in the frequency range 1–30 GHz, which is mainly limited from above by the practically possible values of the applied bias magnetic field necessary to saturate the FM

free layer of the STNO. The introduction of AFMs into current-driven signal generators could raise the generated frequencies to those of the typical range of AFMR frequencies, i.e., to the terahertz range [1,10–12]. In particular, in Ref. [13] it has been theoretically shown that if an AFM material is used as a magnetic layer of a spin Hall auto-oscillator, it would be possible to generate signals with frequencies of 0.1–2.0 THz and amplitudes of approximately 1 V/cm, using driving electric currents that have densities in the range 10^8 – 10^9 A/cm². Note that driving currents of such densities, mainly determined by the magnitude of the easy-plane anisotropy of the AFM, have previously been attained in experiments with STNO devices based on FMs (see, e.g., Ref. [9]). In Ref. [14], it has been shown that the emission power of AFM-based STNOs may reach 1 μ W, which is comparable to that of FM-based STNOs. For the AFM-based STNO from Ref. [13], if we assume that the Pt layer has a height of 10 nm, a length and width of 10 μ m, a resistivity of 10.6×10^{-8} Ω m, and a current density of around 10^8 A/cm², such an emission power corresponds to an efficiency of $\eta \sim 10^{-5}$. This efficiency can be compared to that of FM-based STNOs $\eta \sim 10^{-3}$ [15]. The efficiency of AFM-based STNOs can be increased by using a high- Q subterahertz frequency resonator, such as in

*paavali.popov@gmail.com

†arsafin@gmail.com

Refs. [16] and [17] and as discussed in Ref. [14], and then a subterahertz waveguide [18]. Another way to increase the efficiency is to synchronize an array of STNOs [19].

Another important property of AFMs is the absence of net magnetization in AFM substances, which makes them insensitive to stray dipolar magnetic fields and, therefore, makes the placement of AFM elements in close proximity to each other possible without significant cross-interference in all the possible signal-processing applications. At the same time, this insensitivity of AFMs to external magnetic fields makes it rather difficult to control the magnetization dynamics in AFMs externally.

Of course, there exist means other than external magnetic fields to control the dynamics of magnetization in magnetically ordered substances. It has been shown theoretically that a spin-transfer torque created by a dc current flowing in a layer of a heavy metal (e.g., Pt) adjacent to the AFM layer could reduce the magnetic anisotropy and, therefore, the AFMR frequency in the AFM layer [20], and, at a sufficiently large current magnitude, could excite the terahertz-frequency magnetization dynamics in AFMs [13]. These analytical predictions have recently been confirmed in micromagnetic modeling [21,22]. It has been also confirmed experimentally that an external spin-transfer torque could switch the direction of the AFM order parameter (the Néel vector) in dielectric AFMs [23,24].

Also, it has been shown previously that the magnetization dynamics in ferromagnetic (FM) heterostructures containing piezoelectric and/or multiferroic layers could be controlled by the application of a static electric field across the structure thickness (magnetoelectric and magnetoelastic effects) [25,26]. The application of a transverse voltage (or electric field) creates a stress in the PZ layer, which, due to the magnetoelastic effect in a FM layer, changes the FM-layer magnetization and/or *anisotropy*. The effect of the voltage-induced magnetic anisotropy has been seen in ultrathin FM layers and heterostructures subjected to the action of a perpendicular voltage [27–29]. This effect has been studied in a recent paper [30], where it has been suggested that voltage control can be used to influence the terahertz-frequency magnetization dynamics in AFMs.

In this paper, we apply similar methods to *monocrystalline* AFM, study the influence of the simultaneous application of a transverse dc electric field and a longitudinal dc current to the PZ/AFM/HM layered heterostructure, and evaluate theoretically how such an application can influence the AFM anisotropy and affect the magnetization dynamics in the structure. The studied heterostructure is, in principle, similar to the AFM-based STNOs considered in Refs. [13] and [14], where they are shown as possible terahertz-frequency signal generators. The PZ/AFM stack in our structure corresponds to the AFM layer from Refs. [13] and [14], where it serves as a source of terahertz-frequency dynamics.

We expect that the voltage applied to the PZ layer of the heterostructure will create a stress at the PZ/AFM boundary, which, due to the magnetoelastic effect in AFMs, will create a variation in the AFM anisotropy. This anisotropy variation, in the first approximation, will be linearly proportional to the applied electric field and will depend on the field direction, so that the mechanical stress at the PZ/AFM boundary could either increase or decrease the AFM anisotropy. Since the heterostructure is mainly dielectric, this electric control of the AFM anisotropy could be performed without significant transverse currents that increase dissipation and, since both the AFMR frequency [3–6] and the threshold of the current-induced generation of periodic signals in AFM-based STNOs [13,14] are proportional to the AFM anisotropy, the application of a transverse voltage to the PZ/AFM/HM layered structure could allow us the possibility of tuning the frequency of the AFMR in the subcritical regime. The heterostructure could then be used as a *resonant element* in a passive receiver of terahertz-frequency signals and to reduce the magnitude of the generation threshold, if the heterostructure could be used in the supercritical regime to generate terahertz-frequency periodic signals. The electric control (reduction) of the generation threshold could be of substantial practical importance, as it may help to realize terahertz-frequency generation in AFMs experimentally.

The paper has the following structure. In Sec. I, an introduction to voltage- (or electric-field-) controlled AFM spintronics is presented. In Sec. II, we consider a PZ/AFM bilayer with a transverse electric field applied across the bilayer. In such a situation, we derive a general linear tensorial relation between the vector of the applied electric field and the field-induced change in the AFM anisotropy tensor. In Sec. III, we consider the PZ/AFM/HM layered heterostructure under the simultaneous action of a transverse dc electric field applied to the PZ layer and a longitudinal dc current flowing in the HM layer. Using the approximation of a “sigma model” [6], we derive a general equation describing the magnetization dynamics in the AFM layer, in which the AFM anisotropy is affected by both the external dc current and the external dc electric field. In Sec. IV, we apply the general theory developed above to a particular case of a monocrystalline bianisotropic dielectric AFM—nickel oxide (NiO)—and derive explicit expressions for the AFMR frequency in the subcritical regime, the generation threshold in the critical regime, and the amplitude and frequency of the generated periodic signal in the supercritical regime as functions of the external dc current and the external dc electric field in a particular case in which monocrystalline NiO is used as the AFM material, a lead zirconate titanate-based piezoceramics PZT-5H is used as a PZ material, and Pt is used as a HM. Discussion of the obtained results is presented in Sec. V, while the conclusions are given in Sec. VI.

II. VOLTAGE-CONTROLLED ANISOTROPY IN THIN AFM LAYERS

In this section, we consider the PZ/AFM bilayer shown in Fig. 1, and derive the equations describing the influence of a dc electric field E applied to the PZ layer on the magnetic parameters of the AFM layer. The AFM layer is assumed to be much thinner than the PZ layer, so that it will not affect any of the mechanical properties of the PZ layer. Also, we assume an ideal acoustic contact between the layers, i.e., we assume that the displacement is continuous across the interlayer interface [32]. Here and below, we denote σ_{ij}^{PZ} , e_{ij}^{PZ} and σ_{ij} , e_{ij} as the elastic stress and strain tensors of the PZ and AFM layers, respectively. We also use the Einstein summation convention.

An application of the dc electric field E_k to the PZ layer produces the following strain in the layer:

$$e_{ij}^{\text{PZ}} = d_{ijk}E_k, \quad (1)$$

where d_{ijk} is the strain-piezoelectric tensor of the PZ layer [see Eq. (2.11) in Ref. [33]]. Here, we can use the *bulk* strain-piezoelectric constants of the PZ layer, because the AFM layer is much thinner than the PZ layer. Thus, the mechanical feedback from the AFM layer to the PZ layer is negligible.

The Hooke's law relating the volume stress e_{kl} and strain σ_{ij} induced in the AFM layer can be written as

$$\sigma_{ij} = C_{ijkl}e_{kl}, \quad (2)$$

where C_{ijkl} is the stiffness tensor of the AFM layer.

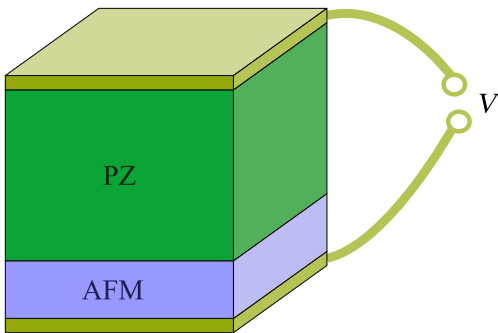


FIG. 1. A schematic view of the considered PZ/AFM bilayer under the influence of a bias electric voltage V : a layer of the AFM material (e.g., NiO) and a layer of the PZ material (e.g., PZT-5H) in a conductive coating. The interface between the AFM and the PZ layers is considered as an ideal acoustic contact. The AFM layer is chosen to be much thinner than the PZ layer, so that the mechanical properties of the PZ layer are not affected by the AFM layer. The conductive coating allows one to apply the transverse electric field E to the PZ layer (such a design has been used in the experimental paper by Sadovnikov *et al.* [31]).

An ideal acoustic contact between the PZ and AFM layers implies that the in-plane strain is continuous across the AFM/PZ interface:

$$P_{ik}e_{kl}^{\text{PZ}}P_{lj} = P_{ik}e_{kl}P_{lj} = e_{ij}^{\text{AF}}, \quad (3)$$

where $P_{ij} = I_{ij} - n_i n_j$ is the projector on the AFM/PZ interface, I_{ij} is the identity matrix, and n_i is the vector normal to the AFM/PZ interface. It should be noted that the net mechanical result of the application of the bias electric voltage (or electric field) to the PZ layer is the creation of the mechanical strain e_{ij}^{AF} at the PZ/AFM interface.

The opposite interface of the AFM layer is considered to be free, so the normal component of the stress σ_{ij} at this interface of the PZ layer should vanish:

$$\sigma_{ij}n_i = 0. \quad (4)$$

To find the components of the strain induced in the AFM layer by the electric field applied to the PZ layer, we need to find the simultaneous solution of the system of Eqs. (2)–(4) comprising the Hooke's law and the two boundary conditions at the boundaries of the AFM layer. In general, the solution of the system of Eqs. (2)–(4) for an arbitrary symmetry of the tensor C_{ijkl} is rather cumbersome. Nonetheless, it can be found in the following general form:

$$e_{ij} = G_{ijkl}e_{kl}^{\text{IF}}. \quad (5)$$

In the case in which the stiffness tensor of the AFM layer C_{ijkl} has a cubic symmetry (as in NiO), the tensor G_{ijkl} in Eq. (5) can be simplified to the following form (see the Appendix):

$$G_{ijkl} = (\delta_{ik}\delta_{jl} - \eta n_i n_j \delta_{kl}), \quad (6)$$

where $\eta = C_{12}/C_{11}$, C_{12} , and C_{11} are the components of the stiffness tensor C_{ijkl} in the Voigt notation. In fact, the existence of strain components dependent on the parameter η is a result of the Poisson effect.

The strain applied to the AFM layer produces the magnetoelastic (ME) energy in this layer, which can be written as [see Eq. (5.66) in Ref. [34]]

$$W^{\text{ME}} = b_{ijkl}m_i^\alpha m_j^\alpha e_{kl}, \quad (7)$$

where b_{ijkl} is the magnetoelastic tensor and m_i^α is the magnetization unit vector of the AFM sublattice, denoted by the index “ α .” The magnetoelastic energy term is quadratic in m_i^α in exactly the same way as the terms describing the first-order magnetocrystalline anisotropy:

$$W^{\text{anis}} = K_{ij}m_i^\alpha m_j^\alpha, \quad (8)$$

where K_{ij} is the tensor of the magnetocrystalline anisotropy.

Therefore, we can formally take into account the magnetoelastic interaction in the AFM layer by introducing the effective magnetic anisotropy tensor containing a magnetoelastic part $K_{ij}^{\text{ME}}(E_f)$ that is dependent on the applied electric field:

$$K_{ij}^{\text{eff}} = K_{ij} + K_{ij}^{\text{ME}}(E_f). \quad (9)$$

This magnetoelastic part of the second-rank AFM anisotropy tensor can be written as

$$K_{ij}^{\text{ME}}(E_f) = b_{ijkl} G_{klpq} (P_{pr} d_{rsf} P_{sq} E_f) = Z_{ijf} E_f. \quad (10)$$

Here, Z_{ijf} is a third-rank tensor, which describes the voltage-induced magnetic anisotropy effect in the AFM layer by linearly coupling the vector of the applied electric field E_f to the second-rank tensor K_{ij}^{ME} of the magnetic anisotropy tensor induced by an applied electric field in an arbitrary direction.

Equations (9) and (10) represent a main general result of this paper, describing how a vectorial external dc electric field E can be used to control the magnetic anisotropy in AFM (and/or FM) materials. The tensor Z_{ijf} describing this effect is defined by the piezoelectric properties of the PZ layer and the magnetoelastic and elastic properties of the AFM layer, as well as by the relative crystallographic orientation of the layers.

It is worth mentioning that in addition to the strain created by the applied electric field, the AFM layer is also affected by the “ground-state” strain caused by the intrinsic interaction between the magnetic and elastic subsystems of the AFM material in the free state (see pp. 173 and 182 in Ref. [35]). The magnetic anisotropy caused by this strain is usually included in the magnetocrystalline anisotropy constants found in the experiments. Thus, we do not consider this effect in any detail here.

III. CURRENT-INDUCED MAGNETIZATION DYNAMICS IN AN AFM HETEROSTRUCTURE BIASED BY A dc ELECTRIC FIELD

The magnetization dynamics in the current-driven AFM/HM bilayer in both the active (generation) [13,14] and the passive (reception) [20] regimes have been discussed previously. In this section, we study the current-driven AFM magnetization dynamics in the PZ/AFM/HM layered heterostructure in the case in which the PZ layer is biased by the dc voltage V (see Fig. 2). In such a structure, the electric current j flowing along the HM layer becomes spin polarized due to the spin Hall effect in the HM, creating a perpendicular spin current. This spin current, polarized along \mathbf{p} , creates a spin-transfer torque (STT) acting on the magnetization sublattices in the AFM layer [13]. The magnetization dynamics in the AFM layer are described by the “sigma-model” equation for the AFM

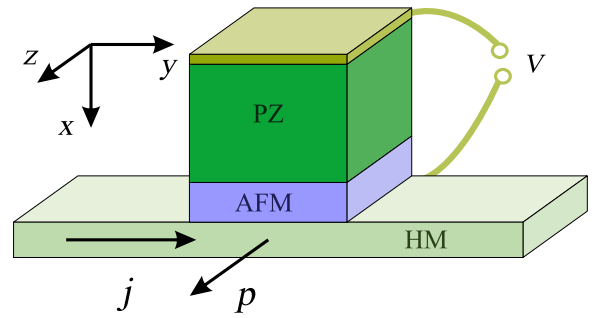


FIG. 2. A schematic view of the three-layer PZ/AFM/HM heterostructure, where the piezoelectric (PZ) layer is biased by the dc voltage V while the layer consisting of a heavy metal (HM) is driven by the longitudinal current of the density j . When the current density in the HM layer exceeds a certain threshold determined by the easy-plane anisotropy in the AFM, the spin-transfer torque created by the current in the HM due to the spin Hall effect generates terahertz-frequency rotation of the magnetization sublattices in the AFM, which can be detected in the HM layer due to the inverse spin Hall effect (for details, see Ref. [13]). The voltage bias applied to the PZ layer can change the anisotropy in the AFM layer and, therefore, the AFMR frequency in the AFM layer in the subcritical (passive) regime, the generation threshold current, and the amplitude of the signal generated in the AFM layer in the supercritical (active) regime.

order parameter—the AFM Néel vector \mathbf{l} [see Eq. (14) in Ref. [13]] which in our case has the following form:

$$\mathbf{l} \times \left(\frac{1}{\omega_{\text{ex}}} \ddot{\mathbf{l}} + \alpha \dot{\mathbf{l}} + \hat{\boldsymbol{\Omega}} \cdot \mathbf{l} + \tau \mathbf{p} \times \mathbf{l} \right) = 0, \quad (11)$$

where $\omega_{\text{ex}} = \gamma H_{\text{ex}}$, γ is the gyromagnetic ratio, H_{ex} is the internal exchange field in the AFM, α is the damping parameter, $\tau = \sigma j$ is the STT strength [13], σ is the electric current to STT proportionality coefficient [13], $\hat{\boldsymbol{\Omega}} = (2\gamma/M_s) \hat{\mathbf{K}}^{\text{eff}}$ is the anisotropy matrix in frequency units, and M_s is the saturation magnetization of the AFM sublattices.

Below, we study the small-amplitude dynamics of the AFM magnetization; therefore, we can represent the Néel vector as $\mathbf{l} = \boldsymbol{\lambda} + \mathbf{s} e^{-i\omega t}$, where $\boldsymbol{\lambda}$ is a static part describing the ground state and \mathbf{s} is the vector describing the excitation, $\boldsymbol{\lambda} \cdot \mathbf{s} = 0$. Using this representation in Eq. (11), we obtain two equations: one describing the static state of the AFM magnetization and the other one describing its small-amplitude dynamics. The “static” equation has the following form:

$$\boldsymbol{\lambda} \times \left(\hat{\boldsymbol{\Omega}} \cdot \boldsymbol{\lambda} + \tau \mathbf{p} \times \boldsymbol{\lambda} \right) = 0, \quad (12)$$

which can be rewritten as

$$\hat{\boldsymbol{\Omega}} \cdot \boldsymbol{\lambda} + \tau \mathbf{p} \times \boldsymbol{\lambda} = h\boldsymbol{\lambda}, \quad (13)$$

where h is the effective static staggered field. The solution to Eq. (12) defines a magnetic equilibrium ground state of Néel vector λ .

The “dynamic” equation can be written in the following form:

$$\lambda \times \left[-\frac{\omega^2}{\omega_{\text{ex}}} \mathbf{s} + (\hat{\Omega} - h\hat{\mathbf{I}}) \cdot \mathbf{s} + \tau \mathbf{p} \times \mathbf{s} \right] = 0. \quad (14)$$

The solution to this “dynamic” equation determines the frequencies of small oscillations around the static equilibrium. Simplifying the above “dynamic” equation, we can rewrite it in the form of a standard eigenvalue problem for the excitation vector \mathbf{s} :

$$\frac{\omega^2}{\omega_{\text{ex}}} \mathbf{s} = \hat{\Omega}_0 \cdot \mathbf{s} + \tau (\lambda \cdot \mathbf{p}) (\lambda \times \mathbf{s}), \quad (15)$$

where

$$\hat{\Omega}_0 = \hat{\mathbf{P}}_\lambda (\hat{\Omega} - h\hat{\mathbf{I}}), \quad (16)$$

$$\hat{\mathbf{P}}_\lambda = \hat{\mathbf{I}} - \lambda \otimes \lambda, \quad (17)$$

and the symbol \otimes denotes a tensor product.

The eigenfrequencies ω can be formally found as solutions to the eigenvalue problem (15). It is important to note that the obtained eigenvalue problem (15) in the case of the AFM dynamics has a form similar to that of a linearized vector Landau-Lifshitz (LL) equation derived in Refs. [36] and [37]. This similarity is natural, because both the sigma-model equation (15) and the linearized LL equations in Refs. [36] and [37] describe the behavior of a unit vector on a sphere.

Equations (12)–(15) represent a general formulation of the problem of the small-amplitude magnetization dynamics in AFMs obtained in the framework of a sigma model and can be used for a wide variety of different AFM crystals and piezoelectrics.

IV. EXAMPLE: VOLTAGE-CONTROLLED DYNAMICS OF A CURRENT-DRIVEN BIANISOTROPIC DIELECTRIC ANTIFERROMAGNET—NiO

To illustrate the general formalism for the AFM magnetization dynamics developed above [Eqs. (12)–(15)], we apply this formalism to the case of a PZT-5H/NiO/Pt layered heterostructure, choosing an AFM crystal (NiO) with cubic symmetry and piezoelectric ceramics PZT-5H polarized in the direction perpendicular to the PZ layer surface ($\mathbf{n} = \mathbf{x}$). The STT in this structure, created by the driving dc current in the Pt layer, is assumed to be polarized along the hard-anisotropy axis of the NiO layer ($\mathbf{p} = \mathbf{z}$).

In such a geometry, the tensor $\hat{\mathbf{K}}^{\text{ME}}$ of the AFM magnetic anisotropy induced by the applied transverse dc voltage V (or the transverse dc electric field E) in the cubic crystal NiO has the form (see the Appendix)

$$\hat{\mathbf{K}}^{\text{ME}} = \begin{pmatrix} -2\eta & 0 & 0 \\ 0 & 1 & 0 \\ 0 & 0 & 1 \end{pmatrix} 2b_1 d_2 E, \quad (18)$$

where d_2 and b_1 are the components of the strain-piezoelectric and the magnetoelastic tensors. The effective magnetic anisotropy tensor $\hat{\Omega}$ for NiO, which contains the magnetocrystalline and induced anisotropies and enters the eigenvalue equation (15), has the form

$$\hat{\Omega} = \omega_h \mathbf{z} \otimes \mathbf{z} - \omega_e \mathbf{y} \otimes \mathbf{y} + \kappa E (-2\eta \mathbf{x} \otimes \mathbf{x} + \mathbf{y} \otimes \mathbf{y} + \mathbf{z} \otimes \mathbf{z}), \quad (19)$$

where $\kappa = 4\gamma b_1 d_2 / M_s$.

Since the ground-state vector λ lies in the x - y plane, it is convenient to represent it in the form $\lambda = \mathbf{x} \sin \phi + \mathbf{y} \cos \phi$. Solving the “static” Eq. (12), we find the angle ϕ determining the equilibrium orientation of the static Néel vector λ ,

$$\phi = \frac{1}{2} \arcsin \frac{2\tau}{\omega_e - \kappa E (1 + 2\eta)}, \quad (20)$$

and the value of the staggered field h ,

$$h = (\kappa E - \omega_e) \cos^2 \phi - 2\eta E \kappa \sin^2 \phi. \quad (21)$$

The solution of the “dynamic” eigenvalue problem (15) yields two AFM eigenmode frequencies:

$$\omega_1 = \sqrt{\omega_{\text{ex}} [\omega_e - \kappa E (1 + 2\eta)] \cos 2\phi}, \quad (22)$$

$$\omega_2 = \sqrt{\omega_{\text{ex}} [\omega_h + \kappa E + (\omega_e - \kappa E) \cos^2 \phi + 2\eta \kappa E \sin^2 \phi]}, \quad (23)$$

which are the frequencies of the lower and higher AFMR modes of the voltage- and current-driven PZT-5H/NiO/Pt layered heterostructure. Since $\omega_h \gg \omega_e$, the influence of the voltage-induced strain and the current-induced STT on the high-frequency mode of the AFMR is negligible. Therefore, in the following we will only discuss in detail the properties of the low-frequency AFMR mode.

Using Eqs. (20) and (22), it is possible to find an explicit expression for the frequency of the low-frequency AFMR mode as a function of the density of the driving current j

and the magnitude of the bias electric field E :

$$\omega_1(j, E) = \sqrt{\omega_{\text{ex}}\omega_{\text{eff}}(E)} \sqrt{1 - \frac{4(\sigma j)^2}{\omega_{\text{eff}}(E)^2}}, \quad (24)$$

where

$$\omega_{\text{eff}}(E) = \omega_e(1 - \beta E) \quad (25)$$

and

$$\beta = \kappa(1 + 2\eta)/\omega_e. \quad (26)$$

The line width $\Delta\omega$ of the found AFMR mode in the small-amplitude approximation does not depend on the magnitudes of j and E and for the intrinsic Gilbert damping parameter is [38]

$$\Delta\omega = \alpha\omega_{\text{ex}} \approx 2\pi \times 18 \text{ GHz}. \quad (27)$$

In the case of $E = 0$ and $j = 0$, it corresponds to the quality factor $Q = \omega/\Delta\omega \approx 12$.

The obtained expression (24) for the frequency of the low-frequency AFMR mode is valid for the values of the driving-current density below the thresholds of the generation regime $j < j_{\text{th}1,2}$ [see Eqs. (4) and (5) in Ref. [13]]. In the absence of the bias electric field ($E = 0$), an equation similar to Eq. (24) has been derived in Eq. (10) in Ref. [20]. In the presence of the electric field, the expressions for the generation thresholds $j_{\text{th}1,2}$ are modified using the replacement $\omega_e \rightarrow \omega_{\text{eff}}(E) = \omega_e(1 - \beta E)$:

$$j_{\text{th}1} = \frac{\omega_e(1 - \beta E)}{2\sigma} = j_{\text{th}0}(1 - \beta E), \quad (28)$$

$$j_{\text{th}2} = \frac{2\alpha}{\pi\sigma} \sqrt{\omega_{\text{ex}}\omega_e(1 - \beta E)}. \quad (29)$$

This means that for the proper sign and magnitude of the bias electric field, the “easy-plane” anisotropy of the AFM can be substantially reduced and, consequently, the threshold of the terahertz-frequency signal generation in a current-driven AFM, which is proportional to the $\omega_e \rightarrow \omega_{\text{eff}}(E)$, can also be reduced.

Unfortunately, this reduction of the generation threshold also leads to a reduction in the amplitude of the generated signal that is proportional to the time derivative of the azimuthal angle of the Néel vector \mathbf{I} in the AFM. In the supercritical (generation) regime [for $j > j_{\text{th}1}(E)$], the expression for the derivative of the azimuthal angle $\dot{\phi}$ has been derived in Eq. (6) in Ref. [13] and for the case of biasing by an electric field E when $\omega_e \rightarrow \omega_{\text{eff}}(E)$, we obtain

$$\dot{\phi} = \frac{\omega(j)}{2} + \frac{\omega_{\text{ex}}\omega_e(1 - \beta E)}{4\sqrt{(\alpha\omega_{\text{ex}})^2 + \omega^2(j)}} \cos \omega(j)t, \quad (30)$$

where $\omega(j) = 2\sigma j/\alpha$.

In our particular case of the PZT-5H/NiO/Pt layered heterostructure, it is possible to calculate all the material coefficients explicitly and we obtain the following value of the coefficient β determining the dependence of the NiO easy-plane anisotropy on the dc electric field applied to the PZT piezoelectric layer: $\beta = 4\gamma b_1 d_2(1 + 2\eta)/\omega_e M_s = 1.64 \times 10^{-2} \text{ (kV/cm)}^{-1}$. In the same structure, the threshold current density of the terahertz-frequency signal generation in the absence of the bias electric field is evaluated as $j_{\text{th}0} = \omega_e/2\sigma = 2.02 \times 10^8 \text{ A/cm}^2$, which is the current density that has been reached in many previous experiments performed in FM-based spin-torque and spin Hall auto-oscillators [7–9].

It should be noted that the magnitude of the coefficient β that quantifies the dependence of the AFM anisotropy on the applied electric field is rather small [approximately $10^{-2} \text{ (kV/cm)}^{-1}$] and that large electric fields, close to those characteristic of dielectric breakdown, are needed to substantially influence the AFM anisotropy and, therefore, all the other properties of an AFM crystal. Thus, for practical applications of the developed formalism, it is very important to find PZ/AFM pairs that have the largest possible coefficient β .

V. DISCUSSION

The results of our study of the influence of the bias dc electric field E applied to the piezoelectric PZ layer and the density j of the driving electric current supplied into the HM layer of the PZ/AFM/HM heterostructure on the magnetic properties of the AFM layer of the same structure are summarized in Figs. 3 and 4.

Figure 3 demonstrates that the application of the dc electric field can, in principle, substantially reduce the AFM anisotropy and, therefore, the threshold current density necessary for the generation of periodic terahertz-frequency signals in current-driven AFM crystals. This result opens a way to the practical development of terahertz-frequency signal generators based on AFM substances. Another notable theoretical result is illustrated in the inset to Fig. 3 and shows that for a sufficiently large bias electric field, the “extinction” threshold current, determined by the Gilbert damping in the AFM crystal [see Eq. (5) in Ref. [13]] could become larger than the “ignition” threshold, determined by the “easy-plane” AFM anisotropy [see Eq. (4) in Ref. [13]] and, therefore, the threshold of generation in AFMs will be determined by the AFM Gilbert damping.

Figure 4 shows the frequency of oscillations in the AFM crystal as a function of the driving current in both the subcritical (passive) and the supercritical (active, or generation) regimes for two values of the electric field. It is clear that in the subcritical regime the frequency of the low-frequency mode of the AFMR is reduced with an increase of the driving current and is also reduced with an increase

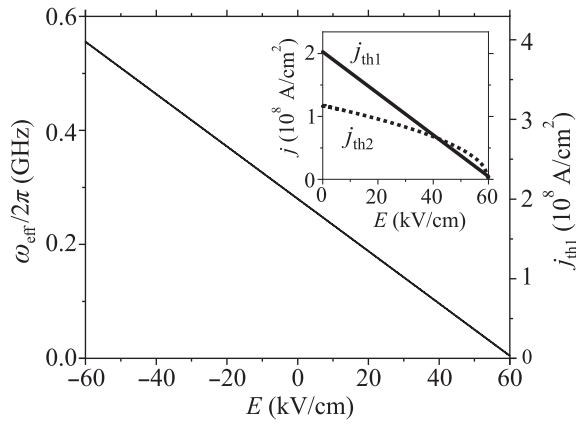


FIG. 3. The dependence of the effective easy-plane anisotropy ω_{eff} (left-hand axis) and the threshold current j_{th1} (right-hand axis) in NiO on the electric field E applied to the PZT layer. Note that both the AFM anisotropy and the generation threshold could be tuned and reduced by the application of an electric field to the PZT layer. The inset demonstrates that for a sufficiently large value of E , the “elimination” threshold j_{th2} can exceed the “ignition” threshold j_{th1} [for details, see Eqs. (4) and (5) in Ref. [13]].

of the applied bias electric field. On the other hand, in the supercritical regime, the frequency of the generated signal is simply proportional to the supplied current density j and is practically independent of the bias electric field E .

Figure 5 again demonstrates that the frequency of the low-frequency AFMR mode in the subcritical(passive) regime is decreased with an increase of the bias electric

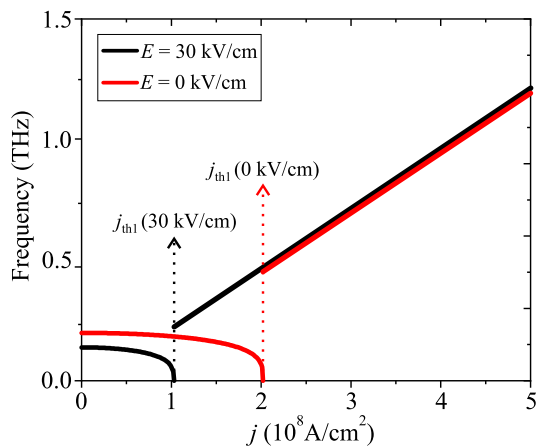


FIG. 4. The dependence of the eigenfrequency of the low-frequency AFMR mode (22) in the passive subcritical ($j < j_{\text{th1}}$) regime and the frequency of generated oscillations $\omega(j)$ in the active supercritical ($j > j_{\text{th1}}$) regime on the density j of the driving electric current, calculated for two values of the electric field E applied to the PZT layer. Note that the AFMR frequency in the subcritical regime is reduced with an increase of the driving-current density j [see also Eq. (10) in Ref. [20]].

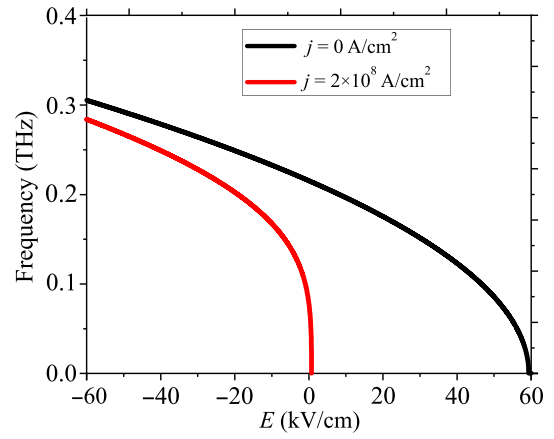


FIG. 5. The dependence of the eigenfrequency of the low-frequency AFMR mode (22) in the passive subcritical regime on the electric field E applied to the PZT layer, calculated for two magnitudes of the driving electric current density j [$j_{1,2} < j_{\text{th1}}(E)$].

field, so that in this regime an AFM crystal biased by a dc electric field can be used as an electrically tunable resonator working at subterahertz frequencies.

Figure 6 shows that the amplitude of the periodic high-frequency signal generated in an AFM in the supercritical regime is reduced both with an increase of the driving-current density and with an increase of the bias electric field. This means that by applying the bias electric field, it is possible to reduce the generation threshold, but the price one will have to pay for this advantage is the reduced amplitude of the generated high-frequency signal.

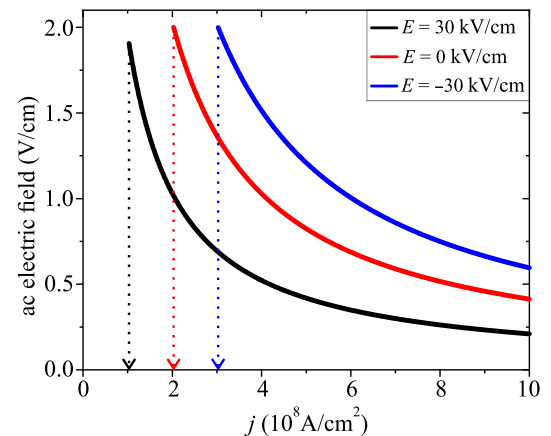


FIG. 6. The dependence of the amplitude of oscillations of the frequency $\omega(j)$ generated in the active supercritical regime on the density j of the driving current for three different values of electric field E applied to the PZT layer. Vertical dashed lines show the position of the generation threshold $j = j_{\text{th1}}(E)$. Note that amplitude of the generated oscillations is reduced with the increase of both the driving current j and the bias electric field E .

Finally, Fig. 7 demonstrates the dynamic behavior of the PZ/AFM/HM layered heterostructure in Fig. 2 under the influence of the dc bias current j and the bias electric field E . Using the dynamic equation (11), we calculate numerically the time dependence of the angular velocity of the AFM Néel vector \mathbf{I} in the (a) subcritical and (b) supercritical regimes. In the subcritical regime [Fig. 7(a)], we assume that the bias current is absent ($j = 0$) and that the magnetization dynamics start when the Néel vector \mathbf{I} is displaced from its equilibrium state ($\mathbf{I} = \lambda$) with the initial condition $\mathbf{I}(t = 0) = \lambda + \mathbf{s}_0$, $\partial\mathbf{I}/\partial t|_{t=0} = 0$. In this case, the magnetization dynamics are described by damped oscillations with a frequency close to the AFMR frequency and this frequency is reduced with an increase of the bias electric field E [see Eq. (24)]. In the supercritical regime [Fig. 7(b)] $j > j_{\text{th1}}(E)$ ($j = 2 \times 10^8$ A/cm²), the dynamics are described by self-sustained oscillations, the frequency of which is determined by the bias current j (for details, see Ref. [13]), while the electric field E determines only the threshold current j_{th1} and the amplitude of the angular-velocity oscillations [see Eq. (30)].

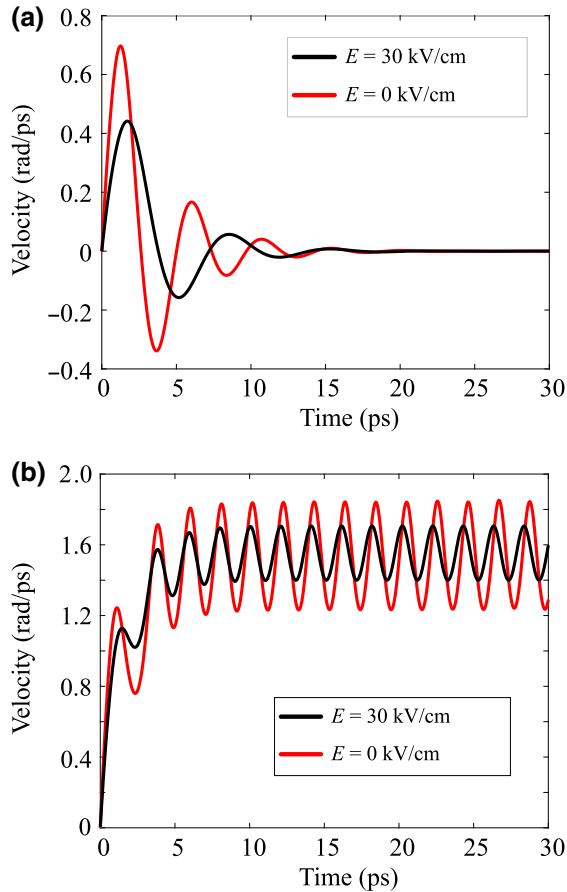


FIG. 7. The numerically calculated dynamical behavior of the PZ/AFM/HM layered heterostructure in Fig. 2 under the influence of a dc bias current and a dc electric field in the (a) subcritical and (b) supercritical regimes. The angular velocity of the rotating AFM Néel vector \mathbf{I} is presented as a function of time.

VI. CONCLUSIONS

The results presented above demonstrate that the dynamic magnetic properties of AFM crystals in PZ/AFM/HM layered heterostructures can be effectively controlled by both the driving current flowing along the HM layer and the transverse dc electric field applied to the PZ layer of the heterostructure.

One of the main results of our current work is the derivation of the general tensorial equations (9) and (10) relating the tensor of anisotropy in an AFM crystal to the vector of the dc electric field applied to the PZ layer. Using these tensorial equations in a particular case of a transverse electric field applied to a NiO AFM crystal (having cubic symmetry), we consider the current-induced dynamics of magnetization in NiO and obtain an expression (25) describing the dependence of the “easy-plane” anisotropy in NiO on the applied dc electric field, and the explicit expression (24) for the frequency of the AFMR acoustic mode as a function of the driving-current density j and the bias electric field E in the subcritical regime $j < j_{\text{th1,2}}$.

We also obtain the expression (30) for the derivative of the azimuthal angle ϕ of the Néel vector \mathbf{I} in the supercritical (generation) regime for $j > j_{\text{th1}}(E)$ in the presence of the bias electric field, which allows us to evaluate the amplitude of the high-frequency signal generated in the AFM layer as a function of j and E (see 6).

We believe that the obtained explicit equations could be used for theoretical analysis in a variety of practical spintronic problems that require AFM-anisotropy manipulation and switching, such as control of magnetic random-access memories (MRAMs) [39,40], the development of terahertz-frequency signal generators [1,12,13] and resonance monochromatic receivers [1,20,22] based on AFM crystals, the control and excitation of spin waves in AFM and FM magnonic devices [41], and many others. The obtained equations can also be useful in the study of the influence of elastic strain on nonmagnetic systems (e.g., Ref. [42]).

ACKNOWLEDGMENTS

This work was supported in part by the U.S. National Science Foundation (Grants No. EFMA-1641989 and No. ECCS-1708982), by the U.S. Air Force Office of Scientific Research under the Grant No. FA9550-19-1-0307, and by the Oakland University Foundation. Studies of the voltage-induced magnetic anisotropy effect were carried out with the support of the Russian Science Foundation (Grant No. 19-19-00607) and a grant from the Government of the Russian Federation for the state support of scientific research conducted under the guidance of leading scientists in Russian higher-education institutions, research institutions, and state research centers of the Russian Federation (Project No. 2019-220-07-9114). Studies of the magnetic dynamics in antiferromagnetic STNOs

with voltage-induced magnetic anisotropy were supported by the Russian Foundation for Basic Research (RFBR) under Grants No. 18-37-20048, No. 18-29-27018, No. 18-57-76001, No. 18-07-00509 A, and No. 18-29-27020, and by the grants of the President of the Russian Federation (Grants No. MK-283.2019.8 and No. MK-3607.2019.9). S.A.N. acknowledges support from the Government of the Russian Federation [Grant No. 074-02-2018-286 for the “Terahertz Spintronics” laboratory of the Moscow Institute of Physics and Technology (MIPT)]. A.R.S. acknowledges the support from the RFBR (Grant No. 19-29-03015).

APPENDIX: MATERIAL CONSTANTS

In this appendix, we present the magnitudes of all the material constants used in the calculations presented above and show explicitly the tensorial formalism leading to the derivation of the general equation (10).

Here, in addition to the quantities σ_{ij}^{PZ} , e_{ij}^{PZ} , σ_{ij} , and e_{ij} defined above, which denote the stress tensors and the elastic strain tensors in the PZ and AFM layers, respectively, we also introduce the quantities σ^{PZ} , e^{PZ} , σ , and e as the six-dimensional vector representations of these tensors in the Voigt notation (see p. 66 in Ref. [33]). We introduce the six-dimensional vectors in order to represent the tensors d_{kij} and C_{ijkl} in more explicit and transparent forms.

In our calculations, we use the following magnetic parameters of the NiO crystal:

$$\begin{aligned} H_e &= 6.2 \times 10^2 \text{ G [38]}, & \omega_e &= \gamma H_e = 2\pi \times 1.75 \text{ GHz}, \\ H_h &= 1.6 \times 10^4 \text{ G [38]}, & \omega_h &= \gamma H_h = 2\pi \times 43.9 \text{ GHz}, \\ H_{\text{ex}} &= 9.8 \times 10^6 \text{ G [38]}, & \omega_{\text{ex}} &= \gamma H_{\text{ex}} = 2\pi \times 27.5 \text{ THz}, \\ M_s &= 3.5 \times 10^2 \text{ Oe [43]}. \end{aligned}$$

The following values of the NiO material constants are taken from Ref. [13]:

$$\begin{aligned} \alpha &= 3.5 \times 10^{-3}; \\ \sigma &= 2\pi \times 4.32 \times 10^{-4} \text{ Hz}/(\text{A}/\text{m}^2). \end{aligned}$$

The following parameters of the ME interaction and components of the NiO stiffness tensor are taken from Ref. [44]:

$$\begin{aligned} W^{\text{ME}} &= b_{ijkl} m_i m_j e_{kl}, & b_{ijkl} &= b_0 \delta_{ij} \delta_{kl} + b_1 (\delta_{ik} \delta_{jl} + \delta_{il} \delta_{jk}), \\ b_0 &= 5.93 \times 10^5 \text{ J}/\text{m}^3, & b_1 &= -17.7 \times 10^5 \text{ J}/\text{m}^3; \\ W^{\text{el}} &= \frac{1}{2} C_{ijkl} e_{ij} e_{kl}, & C_{ijkl} &= C_0 \delta_{ij} \delta_{kl} + C_1 (\delta_{ik} \delta_{jl} + \delta_{il} \delta_{jk}), \\ C_0 &= 7.85 \times 10^{10} \text{ J}/\text{m}^3, & C_1 &= 5.39 \times 10^{10} \text{ J}/\text{m}^3. \end{aligned}$$

In our calculations, we assume that the piezoelectric ceramic PZT-5H is polarized along the x axis (see Fig. 2):

$$\hat{\mathbf{d}} = (\hat{\mathbf{C}}^{\text{PZ}})^{-1} \hat{\mathbf{e}} = \begin{pmatrix} d_1 & 0 & 0 \\ d_2 & 0 & 0 \\ d_2 & 0 & 0 \\ 0 & 0 & 0 \\ 0 & 0 & d_4 \\ 0 & d_4 & 0 \end{pmatrix}, \quad (\text{A1})$$

$$\begin{pmatrix} d_1 \\ d_2 \\ d_4 \end{pmatrix} = \begin{pmatrix} 5.94 \\ -2.75 \\ 7.39 \end{pmatrix} \times 10^{-10} (\text{V}/\text{m})^{-1}, \quad (\text{A2})$$

where $\hat{\mathbf{C}}^{\text{PZ}}$ and $\hat{\mathbf{e}}$ are the stiffness and stress-piezoelectric tensors of PZT-5H, presented on p. 278 in Ref. [33]. Assuming that the dc voltage is applied perpendicular to the interface, so that the dc electric field is directed along the x axis $\mathbf{E} = E\mathbf{x}$, the PZ strain \mathbf{e}^{PZ} can be calculated as

$$\mathbf{e}^{\text{PZ}} = \hat{\mathbf{d}}\mathbf{E} = (d_1, d_2, d_2, 0, 0, 0)^T \times E. \quad (\text{A3})$$

Then, the strain at the PZ/AFM interface \mathbf{e}^{IF} entering Eq. (3) can be represented as

$$\mathbf{e}^{\text{IF}} = P_{ik} e_{kl}^{\text{PZ}} P_{lj} = (0, d_2, d_2, 0, 0, 0)^T \times E. \quad (\text{A4})$$

Let us now explicitly derive the tensor G_{ijkl} for the case of a NiO crystal. The tensor C_{ijkl} , written in the Voigt notation, has the following form:

$$\hat{\mathbf{C}} = \begin{pmatrix} C_{11} & C_{12} & C_{12} & 0 & 0 & 0 \\ C_{12} & C_{11} & C_{12} & 0 & 0 & 0 \\ C_{12} & C_{12} & C_{11} & 0 & 0 & 0 \\ 0 & 0 & 0 & C_{44} & 0 & 0 \\ 0 & 0 & 0 & 0 & C_{44} & 0 \\ 0 & 0 & 0 & 0 & 0 & C_{44} \end{pmatrix}, \quad (\text{A5})$$

$$\begin{pmatrix} C_{11} \\ C_{12} \\ C_{44} \end{pmatrix} = \begin{pmatrix} C_0 + 2C_1 \\ C_0 \\ C_1 \end{pmatrix}. \quad (\text{A6})$$

Then, the boundary condition (4) $\sigma_{ij} n_i = 0$ takes the following explicit form,

$$\begin{cases} C_{12} e_{yy} + C_{12} e_{zz} + C_{11} e_{xx} = 0, \\ 2C_{44} e_{xz} = 0, \\ 2C_{44} e_{xy} = 0, \end{cases} \quad (\text{A7})$$

while the boundary condition (3) $P_{ik} e_{kl} P_{lj} = e_{ij}^{\text{IF}}$ can be written as

$$\begin{cases} e_{yy} = e_{yy}^{\text{PZ}}, \\ e_{zz} = e_{zz}^{\text{PZ}}, \\ 2e_{yz} = 2e_{yz}^{\text{PZ}}. \end{cases} \quad (\text{A8})$$

Taking Eq. (A4) into account, we can rewrite the equation $e_{ij} = G_{ijkl}d_{mkl}E_m$ for NiO in the following form:

$$e_{ij} = \begin{pmatrix} -2\eta & 0 & 0 \\ 0 & 1 & 0 \\ 0 & 0 & 1 \end{pmatrix} d_2 E, \quad (\text{A9})$$

where $\eta = C_{12}/C_{11} = C_0/C_0 + 2C_1$.

We can then obtain an explicit expression for the tensor K_{ij}^{ME} of induced magnetic anisotropy in the form

$$\begin{aligned} K_{ij}^{\text{ME}} &= b_{ijkl}e_{kl} = (b_0\delta_{ij}\delta_{kl} + b_1(\delta_{ik}\delta_{jl} + \delta_{il}\delta_{jk}))e_{kl} \\ &= \begin{pmatrix} -2\eta & 0 & 0 \\ 0 & 1 & 0 \\ 0 & 0 & 1 \end{pmatrix} 2b_1 d_2 E. \end{aligned} \quad (\text{A10})$$

Here, we drop the terms containing b_0 , since their contribution to the ME energy is isotropic. The tensor of magnetocrystalline anisotropy $\hat{\mathbf{K}}$ for NiO has been obtained in Ref. [13] and has the form

$$\hat{\mathbf{K}} = \frac{M_s}{2} \begin{pmatrix} 0 & 0 & 0 \\ 0 & -H_e & 0 \\ 0 & 0 & H_h \end{pmatrix}. \quad (\text{A11})$$

Using the values of the NiO material parameters presented above, we obtain the numerical values of the constants ω_e and β entering Eq. (25) and the constant j_{th0} entering Eq. (28) in the form

$$\omega_e = 2\pi \times 1.75 \text{ GHz}, \quad (\text{A12})$$

$$\beta = \frac{4\gamma b_1 d_2 (1 + 2\eta)}{\omega_e M_s} = 1.64 \times 10^{-2} \text{ (kV/cm)}^{-1}, \quad (\text{A13})$$

$$j_{\text{th0}} = \frac{\omega_e}{2\sigma} = 2.02 \times 10^8 \text{ A/cm}^2. \quad (\text{A14})$$

- [1] O. Gomonay, V. Baltz, A. Brataas, and Y. Tserkovnyak, Antiferromagnetic spin textures and dynamics, *Nat. Phys.* **14**, 213 (2018).
- [2] M. B. Jungfleisch, W. Zhang, and A. Hoffmann, Perspectives of antiferromagnetic spintronics, *Phys. Lett. A* **382**, 865 (2018).
- [3] A. F. Andreev and V. I. Marchenko, Symmetry and the macroscopic dynamics of magnetic materials, *Sov. Phys. Usp.* **23**, 21 (1980).
- [4] A. Kosevich, B. Ivanov, and A. Kovalev, Magnetic solitons, *Phys. Rep.* **194**, 117 (1990).
- [5] I. Affleck and R. A. Weston, Theory of near-zero-wave-vector neutron scattering in Haldane-gap antiferromagnets, *Phys. Rev. B* **45**, 4667 (1992).

- [6] B. A. Ivanov, Spin dynamics of antiferromagnets under action of femtosecond laser pulses (review article), *Low Temp. Phys.* **40**, 91 (2014).
- [7] L. Liu, T. Moriyama, D. C. Ralph, and R. A. Buhrman, Spin-Torque Ferromagnetic Resonance Induced by the Spin Hall Effect, *Phys. Rev. Lett.* **106**, 036601 (2011).
- [8] M. Collet, X. de Milly, O. d'Allivy Kelly, V. V. Naletov, R. Bernard, P. Bortolotti, J. Ben Youssef, V. E. Demidov, S. O. Demokritov, J. L. Prieto *et al.*, Generation of coherent spin-wave modes in yttrium iron garnet microdiscs by spin-orbit torque, *Nat. Commun.* **7**, 10377 (2016).
- [9] Z. Duan, A. Smith, L. Yang, B. Youngblood, J. Lindner, V. E. Demidov, S. O. Demokritov, and I. N. Krivorotov, Nanowire spin torque oscillator driven by spin orbit torques, *Nat. Commun.* **5**, 5616 (2014).
- [10] H. V. Gomonay and V. M. Loktev, Spin transfer and current-induced switching in antiferromagnets, *Phys. Rev. B* **81**, 144427 (2010).
- [11] E. V. Gomonay and V. M. Loktev, Spintronics of antiferromagnetic systems (review article), *Low Temp. Phys.* **40**, 17 (2014).
- [12] R. Cheng, D. Xiao, and A. Brataas, Terahertz Antiferromagnetic Spin Hall Nano-Oscillator, *Phys. Rev. Lett.* **116**, 207603 (2016).
- [13] R. Khymyn, I. Lisenkov, V. Tiberkevich, B. A. Ivanov, and A. Slavin, Antiferromagnetic THz-frequency Josephson-like oscillator driven by spin current, *Sci. Rep.* **7**, 43705 (2017).
- [14] O. R. Sulymenko, O. V. Prokopenko, V. S. Tiberkevich, A. N. Slavin, B. A. Ivanov, and R. S. Khymyn, Terahertz-Frequency Spin Hall Auto-Oscillator Based on a Canted Antiferromagnet, *Phys. Rev. Appl.* **8**, 064007 (2017).
- [15] K. D. Sattler, *Handbook of Nanophysics: Functional Nanomaterials* Handbook of Nanophysics (CRC Press, New York, 2010).
- [16] N. Ginzburg, A. Malkin, A. Sergeev, S. Fil'chenkov, and V. Zaslavsky, Highly selective surface-wave resonators for terahertz frequency range formed by metallic Bragg gratings, *Phys. Lett. A* **382**, 925 (2018).
- [17] C. Mathai, R. Jain, V. G. Achanta, S. P. Duttgupta, D. Ghindani, N. R. Joshi, R. Pinto, and S. S. Prabhu, Sensing at terahertz frequency domain using a sapphire whispering gallery mode resonator, *Opt. Lett.* **43**, 5383 (2018).
- [18] M. Navarro-Cía, J. Wu, H. Liu, and O. Mitrofanov, Generation of radially-polarized terahertz pulses for coupling into coaxial waveguides, *Sci. Rep.* **6**, 38926 (2016).
- [19] M. Zahedinejad, A. A. Awad, S. Muralidhar, R. Khymyn, H. Fulara, H. Mazraati, M. Dvornik, and J. Åkerman, Two-dimensional mutually synchronized spin Hall nano-oscillator arrays for neuromorphic computing, *Nat. Nanotechnol.* **15**, 47 (2020).
- [20] I. Lisenkov, V. Tyberkevych, and A. Slavin, in *Proceedings of 62nd MMM Conference* (Pittsburgh, USA, 2017).
- [21] V. Puliafito, R. Khymyn, M. Carpentieri, B. Azzarboni, V. Tiberkevich, A. Slavin, and G. Finocchio, Micromagnetic modeling of terahertz oscillations in an antiferromagnetic material driven by the spin Hall effect, *Phys. Rev. B* **99**, 024405 (2019).
- [22] V. Puliafito, I. Medlej, I. Lisenkov, author M. Carpentieri, B. Azzarboni, A. Slavin, and G. Finocchio, in *Proceedings of MMM-2019 Conference* (Las Vegas, USA, 2019).

- [23] P. Wadley, B. Howells, J. Železný, C. Andrews, V. Hills, R. P. Campion, V. Novák, K. Olejník, F. Maccherozzi, S. S. Dhesi *et al.*, Electrical switching of an antiferromagnet, *Science* **351**, 587 (2016).
- [24] L. Baldrati, O. Gomonay, A. Ross, M. Filianina, R. Lebrun, R. Ramos, C. Leveille, F. Fuhrmann, T. R. Forrest, F. Maccherozzi, S. Valencia, F. Kronast, E. Saitoh, J. Sinova, and M. Kläui, Mechanism of Néel Order Switching in Antiferromagnetic Thin Films Revealed by Magnetotransport and Direct Imaging, *Phys. Rev. Lett.* **123**, 177201 (2019).
- [25] G. Srinivasan, E. T. Rasmussen, B. J. Levin, and R. Hayes, Magnetoelectric effects in bilayers and multilayers of magnetostrictive and piezoelectric perovskite oxides, *Phys. Rev. B* **65**, 134402 (2002).
- [26] C.-W. Nan, M. I. Bichurin, S. Dong, D. Viehland, and G. Srinivasan, Multiferroic magnetoelectric composites: Historical perspective, status, and future directions, *J. Appl. Phys.* **103**, 031101 (2008).
- [27] S. Sahoo, S. Polisetty, C.-G. Duan, S. S. Jaswal, E. Y. Tsymbal, and C. Binek, Ferroelectric control of magnetism in BaTiO₃/Fe heterostructures via interface strain coupling, *Phys. Rev. B* **76**, 092108 (2007).
- [28] F. Zighem, D. Faurie, S. Mercone, M. Belmeguenai, and H. Haddadi, Voltage-induced strain control of the magnetic anisotropy in a Ni thin film on flexible substrate, *J. Appl. Phys.* **114**, 073902 (2013).
- [29] M. Staruch, D. B. Gopman, Y. L. Iunin, R. D. Shull, S. F. Cheng, K. Bussmann, and P. Finkel, Reversible strain control of magnetic anisotropy in magnetoelectric heterostructures at room temperature, *Sci. Rep.* **6**, 37429 (2016).
- [30] A. Barra, J. Domann, K. W. Kim, and G. Carman, Voltage Control of Antiferromagnetic Phases at Near-Terahertz Frequencies, *Phys. Rev. Appl.* **9**, 034017 (2018).
- [31] A. V. Sadovnikov, A. A. Grachev, S. E. Sheshukova, Y. P. Sharaevskii, A. A. Serdobintsev, D. M. Mitin, and S. A. Nikitov, Magnon Straintronics: Reconfigurable Spin-Wave Routing in Strain-Controlled Bilateral Magnetic Stripes, *Phys. Rev. Lett.* **120**, 257203 (2018).
- [32] B. Auld, *Acoustic Fields and Waves in Solids*, A Wiley-Interscience Publication (Wiley, New York, 1973).
- [33] J. Yang, *An Introduction to the Theory of Piezoelectricity* (Springer International Publishing, New York, 2006).
- [34] E. Turov, A. Kolchanov, V. Men'shenin, I. Mirsaev, and V. Nikolaev, *Symmetry and Physical Properties of Antiferromagnets* (Fizmatlit, Moscow, 2001).
- [35] G. Krinichik, *Physics of Magnetic Phenomena* (Moscow University Press, Moscow, 1976).
- [36] R. Verba, G. Melkov, V. Tiberkevich, and A. Slavin, Collective spin-wave excitations in a two-dimensional array of coupled magnetic nanodots, *Phys. Rev. B* **85**, 014427 (2012).
- [37] I. Lisenkov, V. Tyberkevych, S. Nikitov, and A. Slavin, Theoretical formalism for collective spin-wave edge excitations in arrays of dipolarly interacting magnetic nanodots, *Phys. Rev. B* **93**, 214441 (2016).
- [38] A. J. Sievers and M. Tinkham, Far infrared antiferromagnetic resonance in MnO and NiO, *Phys. Rev.* **129**, 1566 (1963).
- [39] T. Nozaki, M. Endo, M. Tsujikawa, T. Yamamoto, T. Nozaki, M. Konoto, H. Ohmori, Y. Higo, H. Kubota, A. Fukushima *et al.*, Voltage-controlled magnetic anisotropy in an ultrathin Ir-doped Fe layer with a CoFe termination layer, *APL Mater.* **8**, 011108 (2020).
- [40] X. Chen, X. Zhou, R. Cheng, C. Song, J. Zhang, Y. Wu, Y. Ba, H. Li, Y. Sun, Y. You *et al.*, Electric field control of Néel spin-orbit torque in an antiferromagnet, *Nat. Mater.* **18**, 931 (2019).
- [41] B. Rana and Y. Otani, Towards magnonic devices based on voltage-controlled magnetic anisotropy, *Commun. Phys.* **2**, 90 (2019).
- [42] D. S. Ponomarev, A. Gorodetsky, A. E. Yachmenev, S. S. Pushkarev, R. A. Khabibullin, M. M. Grekhov, K. I. Zaytsev, D. I. Khusyainov, A. M. Buryakov, and E. D. Mishina, Enhanced terahertz emission from strain-induced InGaAs/InAlAs superlattices, *J. Appl. Phys.* **125**, 151605 (2019).
- [43] M. T. Hutchings and E. J. Samuelsen, Measurement of spin-wave dispersion in NiO by inelastic neutron scattering and its relation to magnetic properties, *Phys. Rev. B* **6**, 3447 (1972).
- [44] T. Nussle, P. Thibaudeau, and S. Nicolis, Coupling magneto-elastic Lagrangians to spin transfer torque sources, *J. Magn. Magn. Mater.* **469**, 633 (2019).

Correction: Typographical errors were found in Eq. (15), Eq. (16), and in the inline equation before Eq. (20) and have been fixed.